ISSN: 3007-9640 DOI: https://doi.org/10.70114/acmsr.2026.8.1.P1

Assessments of Ground Subsidence and Stability Along G218 Highway at Xinjiang Uygur Autonomous Region, China, between 2022 and 2024 with Sentinel-1 Data

Guanwei Jia [1, a],Yangqi Gao [2, b], Chuanguang Zhu [2, c] and Maoyuan Nan [2, d*]

[1] China Energy Shuohuang Railway Development Co., Ltd., Suning, 062350, China;

[2] Hunan University of Science and Technology, Xiangtan, 411201, China.

[a] 312581570@qq.com, [b] 931766719@qq.com, [c] zhucg@hnust.edu.cn, [d] 379412301@qq.com

Abstract. Highway G218, the world's longest brick-paved road, serves as a vital transportation corridor connecting northern and southern Xinjiang Uygur Autonomous Region. However, it traverses permafrost regions and is exposed to a range of extreme climatic conditions. To ensure the safe and reliable operation of this highway, continuous deformation monitoring is essential. Multi-temporal InSAR (MT-InSAR) can monitor the ground deformation with high-resolution over a large area, thereby overcoming the spatiotemporal limitations of conventional *in-situ* measurements. In this paper, 82 Sentinel-1A images acquired from January 2022 to September 2024 were utilized, integrating persistent scatterers (PS) and distributed scatterers (DS) to perform MT-InSAR deformation monitoring along the Nalati–Baluntai section of G218. The results indicate that, during the study period, the surface deformation rates along the highway primarily ranged between −2 and 5 mm/yr, with the maximum rate of 16 mm/yr, indicating that the ground surface is relatively stable. Notably, the observed deformation is associated with two environmental factors: precipitation fluctuations and soil frost heave effects induced by changes in surface temperature.

Keywords: InSAR;persistent scatterer; distributed scatterer; highway; ground deformation; stabiligy.

1. Introduction

By the end of 2024, China's highway network had reached 5.49 million km, making its stability and safety critical to both transportation efficiency and public safety. The Nalati–Baluntai section of National Highway G218 crosses permafrost regions of the Tianshan Mountains and an active seismic zone, where severe cold, high altitude, avalanches, and complex geological conditions jointly increase the risk of structural instability. Under such conditions, continuous deformation monitoring is essential for the early detection of potential hazards and for supporting reliable early warning systems.

Conventional deformation monitoring techniques, such as leveling and the Global Positioning System (GPS), provide high accuracy but are constrained by sparse spatial sampling, high operational costs, and limited temporal resolution. These limitations become particularly pronounced in large-scale, linear infrastructure systems (e.g., highways), where dense, continuous, and long-term observations are required.

Synthetic Aperture Radar Interferometry (InSAR) offers a compelling alternative by enabling large-scale, high-resolution surface deformation monitoring independent of weather and illumination conditions. By exploiting the phase information of radar signals, InSAR can retrieve both topographic and deformation signals with high precision [1-3]. However, conventional InSAR techniques remain challenged by temporal and spatial decorrelation, as well as atmospheric disturbances, which can significantly degrade measurement accuracy [4]. Multi-temporal InSAR (MT-InSAR) mitigate the effects of temporal and spatial decorrelation by exploiting persistent scatterers (PS). Specifically, differential interferometric analysis of multi-temporal SAR images enables the identification of scatterers exhibiting stable scattering behavior over multiple acquisitions, thereby facilitating reliable extraction of surface deformation information [5, 6].

ISSN: 3007-9640 DOI: https://doi.org/10.70114/acmsr.2026.8.1.P1

Nevertheless, in rural areas characterized by vegetation cover or bare soil, where man-made targets are scarce, conventional time-series InSAR methods based on high-coherence point targets often yield insufficient monitoring points, limiting their ability to capture the spatial variability of deformation. To address this limitation, MT-InSAR approaches incorporating DS have been introduced [7]. However, DS remain highly susceptible to temporal and spatial decorrelation, resulting in a low signal-to-noise ratio. Consequently, statistically homogeneous pixels (SHP) are typically employed to re-estimate the DS phase. Conventional DS phase estimation methods, such as the phase triangulation algorithm (PTA) [7, 8] and eigenvalue decomposition (EVD) [9, 10], are computationally intensive, a limitation that becomes increasingly significant with the growing availability of high spatiotemporal resolution SAR data [11, 12]. To address this challenge, this study introduces a power method-based strategy, which estimates the dominant eigenvalue and its corresponding eigenvector through efficient matrix–vector operations, thereby significantly improving computational efficiency. By integrating PS and DS within a unified time-series InSAR framework for deformation monitoring along the Nalati–Baluntai section of National Highway G218 in Xinjiang Uygur Autonomous Region, the spatial density of coherent points is significantly increased. Subsequently, the bootstrap method is employed to assess monitoring accuracy, and the driving factors of deformation are further analyzed in relation to precipitation and surface temperature variations.

2. Study area and SAR dataset

2.1 Study area

Highway G218 was constructed in the late 1950s and fully renovated in 2001. Located in the Tianshan Mountains, it extends from Horgos City in the Xinjiang Uygur Autonomous Region to Ruoqiang County on the border with Qinghai Province. The highway, also known as the Horgos–Ruoqiang Highway (Huoluo Line), has a total length of 1,189 km and passes through Yining, Gongnaisi, Baluntai, and Korla. It is recognized as the world's longest brick-paved national highway connecting Xinjiang with neighboring regions. This study focuses on the Nalati–Baluntai section, which is approximately 215 km long, extending from 84°26′ E to 85°72′ E and 43°11′ N to 43°28′ N. The location of the study area is shown in Fig. 1.

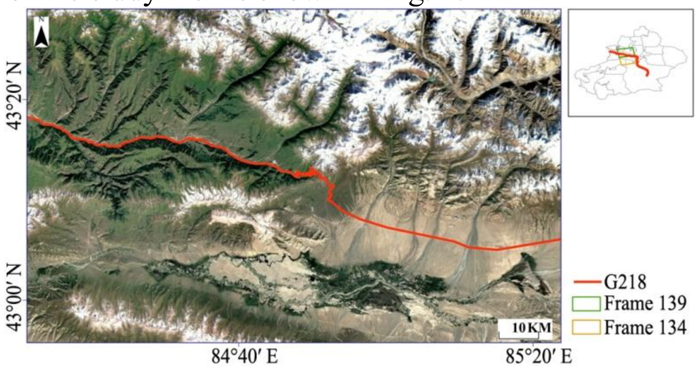

Fig. 1 Location of study area

Situated in the hinterland of the Tianshan Mountains, the study area is characterized by complex topography, with elevations generally higher in the south and lower in the north. The altitude ranges from approximately 1,000 m in river valleys to over 3,500 m in alpine regions, with portions of the Nalati Mountains exceeding this elevation. The highway traverses multiple mountain canyons and is subjected to adverse environmental conditions, including frequent crosswinds, high altitude, severe cold, hypoxia, and permafrost. Geologically, the study area lies within the convergence zone between the Tarim Plate and the Yili Plate, where faults and folds are well developed, leading to a highly complex structural setting. The region has undergone multiple phases of tectonic deformation. Climatically, it experiences long, cold winters and hot, dry summers with significant

ISSN: 3007-9640 DOI: https://doi.org/10.70114/acmsr.2026.8.1.P1

precipitation. Long-term tectonic activity and fluvial erosion have formed deep canyons, featuring alternating ridges and gullies as well as steep slopes.

2.2 SAR dataset

The SAR imagery used in this study were acquired by Sentinel-1A satellite operated by the European Space Agency (ESA). Sentinel-1A, launched on April 3, 2014, is equipped with a C-band SAR sensor, operates at an altitude of approximately 690 km, and has a revisit cycle of 12 days, providing a spatial resolution of about 5 m × 20 m. A total of 82 Sentinel-1A images in ascending mode were collected between January 2022 and September 2024. The corresponding spatiotemporal interferometric baselines are illustrated in Fig. 2.

The DEM used in this study consist of the 30 m resolution Copernicus Digital Elevation Model (COP-DEM), which was employed to remove the topographic phase. For orbit correction, high-precision Precise Orbit Ephemerides (POD) provided by ESA were used to mitigate orbital errors in the Sentinel-1 data.

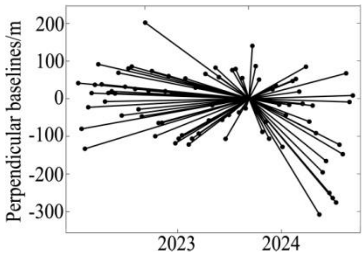

Fig. 2 Connected network of interferograms. Black dots and grey lines denote the Sentinel-1 acquisitions and interferograms, respectively.

3. Methodology

Given the limited availability of PS in the study area, this study integrates PS and DS for surface deformation monitoring along Highway G218. A SAR image acquired on August 23, 2023, was selected as the reference image. The SAR image stack was first preprocessed through coregistration and resampling [13], followed by azimuth and range spectral filtering to mitigate Doppler centroid frequency shifts. Subsequently, targets exhibiting stable backscattering behavior were identified as preliminary PS candidates using the amplitude dispersion threshold method. After phase stability analysis, points exhibiting high phase coherence were retained as the final PS set. A time-series intensity dataset was subsequently generated. A predefined window size and statistical threshold were used to identify statistically homogeneous pixels (SHP) and derive initial DS candidates. Phase optimization for DS targets was conducted using the time-series phases of the SHP. Specifically, the covariance matrix of the homogeneous pixels was decomposed via EVD, and the eigenvector corresponding to the largest eigenvalue was adopted as the optimized phase. The conventional EVD approaches are computationally intensive [11, 12]. To address this challenge, we estimate the DS phase using power method which can saves about 60% to 80% computation time. Further details can be found in [11]. A temporal coherence threshold was then applied to retain DS points with phase quality exceeding the predefined threshold. The PS and DS points were subsequently integrated to form a unified set of coherent targets. Surface deformation was then estimated using the StaMPS software package [14, 15].

4. Results and discussion

4.1 InSAR deformation accuracy analysis

In the absence of *in-situ* measurements, such as leveling or GNSS observations, the bootstrap method was employed to assess the accuracy of the InSAR-derived deformation results, as illustrated in Fig. 3. The analysis shows that the standard deviations of most coherent points

ISSN: 3007-9640 DOI: https://doi.org/10.70114/acmsr.2026.8.1.P1
primarily range between 3 and 4 mm/yr. Higher standard deviations are observed in the southeastern part of the study area, whereas the northwestern region exhibits lower values, indicating that the estimated deformation rates in this area are more stable. Even in regions with relatively higher variability, the standard deviation remains below 5 mm/yr. Overall, these results demonstrate that the deformation estimates derived from coherent points in this study exhibit good accuracy and reliability.

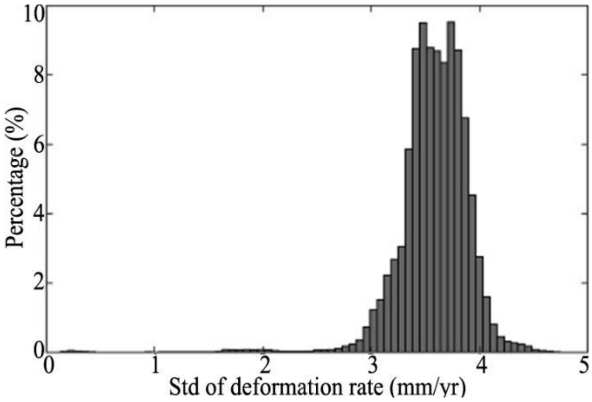

Fig. 3 Distribution of the standard deviation of InSAR-derived deformation rate.

4.2 Spatiotemporal Characteristics of Deformation

During PS processing, the amplitude dispersion threshold was set to 0.4 for preliminary PS selection, and pixels with coherence greater than 0.5 were retained as final PS points. For DS processing, a sliding window of 9 × 35 pixels was adopted to identify statistically homogeneous pixels, with a minimum size of 30. The DS phase was efficiently estimated using the power method (PM) [14], with a goodness-of-fit threshold of 0.7. Subsequently, PS and DS points were integrated into a unified set of coherent targets for time-series InSAR analysis.

The deformation results within a 2-km buffer zone on both sides of National Highway G218 are illustrated in Fig. 4. The average deformation rates along the G218 corridor range from −10 mm/yr to 15 mm/yr, with no evident large-scale subsidence features. In the western mountainous region, coherent targets are sparsely distributed and mainly located along the road. In contrast, the eastern region is characterized by gentle terrain, where coherent targets are significantly denser and exhibit smaller variations in deformation rates.

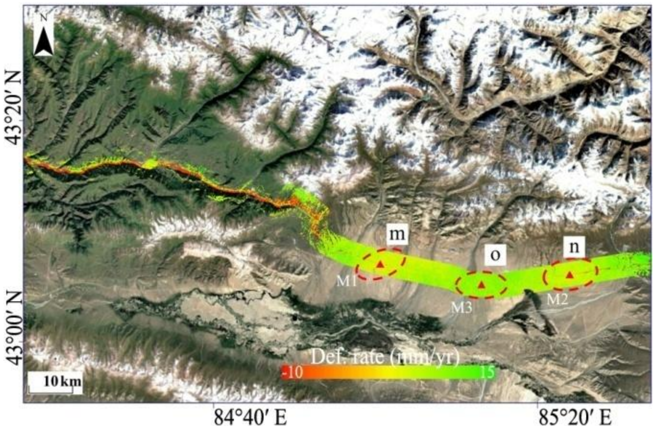

Fig. 4 The average deformation rates of ground along G218.

To further illustrate the spatial distribution of deformation, a deformation profile along the highway is presented in Fig. 5. The results indicate that the deformation rates along the route primarily range between −2 mm/yr and 5 mm/yr, suggesting that most sections of the highway remain relatively stable.

ISSN: 3007-9640 DOI: https://doi.org/10.70114/acmsr.2026.8.1.P1

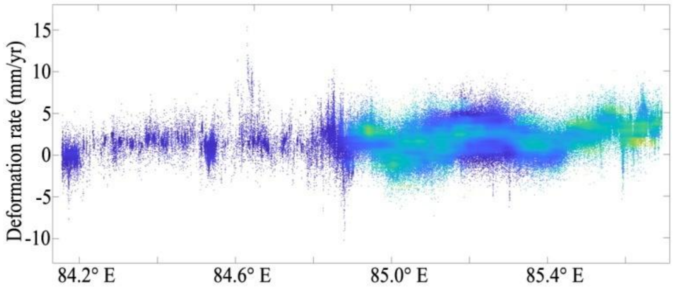

Fig. 5 The profile of average deformation rates along G218.

4.3 Cause analysis

To investigate the temporal deformation characteristics along Highway G218, three targets (M1, M2, and M3) were selected. The potential driving factors were analyzed by integrating precipitation and ground temperature data, as shown in Fig. 6. The cumulative displacement trends of the three targets are broadly consistent and exhibit nonlinear behavior. The displacement shows a gradual increase over time, remaining below 10 mm.

Notable changes in displacement trends are observed around September 2022 and September 2023, which may be associated with increased precipitation. Although these variations affect the cumulative displacement, the overall deformation magnitude remains small. In contrast, pronounced fluctuations occur around January 2023 and January 2024, which are likely related to frost heave induced by temperature variations (Fig. 6(b)), as well as potential external disturbances such as construction activities.

Analysis of optical imagery indicates that engineering infrastructure is sparsely distributed along the highway, with limited human activity and no evident large-scale agricultural or industrial development. This suggests that the observed deformation is minimally influenced by anthropogenic factors and is primarily controlled by natural processes. The observed minor deformation fluctuations are primarily associated with precipitation variability and temperature-driven frost heave effects (Fig. 6). Frost heave, resulting from the expansion and contraction of seasonally frozen soil during temperature fluctuations, can induce subtle surface deformation, particularly in areas with higher soil moisture. In addition, given the complex topographic and geological conditions, surface water flow may further contribute to localized short-term deformation.

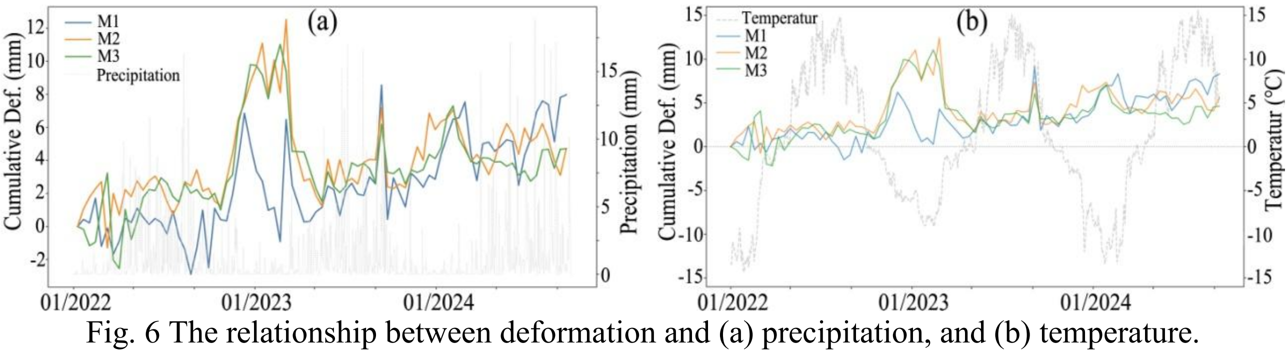

Fig. 6 The relationship between deformation and (a) precipitation, and (b) temperature.

5. Conclusion

Based on 82 Sentinel-1 SAR images, this study applied a MT-InSAR approach integrating PS and DS to monitor surface deformation and assess the stability of the Nalati–Baluntai section of National Highway G218. By combining the complementary strengths of PS and DS targets, a high-density set of coherent points was constructed, enabling the retrieval of the time-series deformation rate field of the study area. The results indicate that deformation rates within a 2-km buffer zone along the G218 corridor primarily range between −2 mm/yr and 5 mm/yr, suggesting that the ground surface in this section is generally stable.

ISSN: 3007-9640 DOI: https://doi.org/10.70114/acmsr.2026.8.1.P1

Analysis of cumulative displacements at representative points, together with precipitation and temperature data, shows that the deformation exhibits nonlinear temporal behavior and is correlated with environmental variations. Deformation fluctuations were more pronounced around September 2022 and September 2023, likely associated with increased precipitation or external disturbances. In contrast, the uplift observed around January 2023 and January 2024 is attributed to frost heave induced by temperature fluctuations.

Overall, surface deformation along this highway section remains stable, with minor variations primarily associated with precipitation changes and temperature-driven freeze–thaw processes. Future work should focus on continuous monitoring and the integration of multi-source data to further enhance deformation analysis and prediction capabilities, thereby providing a more robust basis for the safety assessment of critical infrastructure.

Acknowledgements

The authors acknowledge the developers of the StaMPS software, which is available at http://homepages.see.leeds.ac.uk/~earahoo/stamps/index.html. The authors also acknowledge the European Space Agency (ESA) for providing the Sentinel-1A SAR and DEM data. This work is supported by the Science and Technology Innovation Project of China Energy Group (Grant No. GJNY-23-164).

References

[1] Gabriel, A. K., Goldstein, R. M., and Zebker, H. A. Mapping Small Elevation Changes over Large Areas: Differential Radar Interferometry. Journal of Geophysical Research, 1989, 94: 9183-9191.

[2] Zhu Chuanguang, Wu Wenhao, Motagh M, et al. Assessments of land subsidence along the Rizhao-Lankao high-speed railway at Heze, China, between 2015 and 2019 with Sentinel-1 data. Natural Hazards and Earth System Science, 2020, 20: 3399-3411.

[3] Jiang Zhuo, Shi Guoqiang, Wu Songbo, et al. Unveiling multimodal consolidation process of the newly reclaimed HKIA 3rd runway from satellite SAR interferometry, ICA analytics and Terzaghi consolidation theory. Remote Sensing of Environment, 2025, 318: 114561.

[4] Ma Z. F., Liu J. H., Yosuke A, et al. Towards big SAR data era: An efficient Sentinel-1 Near-Real-Time InSAR processing workflow with an emphasis on co-registration and phase unwrapping. ISPRS Journal of Photogrammetry and Remote Sensing, 2022, 188: 286-300.

[5] Ferretti, A., Prati, C., and Rocca, F.: Non-linear Subsidence Rate Estimation Using Permanent Scatterers in Differential SAR Interferometry, IEEE Transactions on Geoscience and Remote Sensing, 2000, 38(5), 2202-2212.

[6] Ferretti A, Prati C, Rocca F. Permanent scatterers in SAR interferometry. IEEE Transactions on geoscience and remote sensing, 2001, 39(1): 8-20.

[7] Ferretti A, Fumagalli A, Novali F, et al. A new algorithm for processing interferometric data-stacks: SqueeSAR. IEEE transactions on geoscience and remote sensing, 2011, 49(9): 3460-3470.

[8] Samiei-Esfahany S, Martins J E, Van Leijen F, et al. Phase estimation for distributed scatterers in InSAR stacks using integer least squares estimation. IEEE Transactions on Geoscience and Remote Sensing, 2016, 54(10): 5671-5687.

[9] Fornaro G, Verde S, Reale D, et al. CAESAR: An approach based on covariance matrix decomposition to improve multibaseline-multitemporal interferometric SAR processing. IEEE Transactions on Geoscience and Remote Sensing, 2014, 53(4): 2050-2065.

[10] Ansari H, De Zan F, Bamler R. Efficient phase estimation for interferogram stacks. IEEE Transactions on Geoscience and Remote Sensing, 2018, 56(7): 4109-4125.

[11] Zhu Chuanguang, Gao Yangqi, Zhang Liya, et al. Fast phase estimation approach for distributed scatterer based on power method. IEEE journal of selected topics in applied earth observations and remote sensing, 2025, 18: 12819.

ISSN: 3007-9640 DOI: https://doi.org/10.70114/acmsr.2026.8.1.P1
[12] Wang D., Even M., Kutterer H. Deep learning based distributed scatterers acceleration approach: Distributed scatterers prediction Net. International Journal of Applied Earth Observation and Geoinformation, 2022, 115: 103112.

[13] Yague-Martinez, N., Prats-Iraola, P., Rodriguez, G. F., et al. Interferometric Processing of Sentinel-1 TOPS Data. IEEE Transactions on Geoscience and Remote Sensing, 2016, 54(4): 2220-2234.

[14] Hooper, A., Zebker, H. Phase unwrapping in three dimensions with application to InSAR time series. Journal of Optical Society of America, 2007, 24: 2737-2747.

[15] Hooper, A., Segall, P., Zebker, H. Persistent Scatterer Interferometric Synthetic Aperture Radar for Crustal Deformation Analysis, with Application to Volcán Alcedo, Galápagos. Journal of Geophysical Research, 2007, 112: B07407.